

An improved semi-Lagrangian time splitting spectral method for the semi-classical Schrödinger equation with vector potentials using NUFFT

Zheng MA^a, Yong ZHANG^{b,c,*}, Zhennan ZHOU^d

^aDepartment of Mathematics, Shanghai Jiao Tong University, 800 Dongchuan RD, Shanghai, 200240, China

^bUniversité de Rennes 1, IRMAR, Campus de Beaulieu, 35042 Rennes Cedex, France

^cWolfgang Pauli Institute c/o Fak. Mathematik, University Wien, Oskar-Morgenstern-Platz 1, 1090 Vienna, Austria

^dDepartments of Mathematics, Duke University, Box 90320, Durham, NC, 27708, USA

Abstract

In this paper, we propose a new time splitting Fourier spectral method for the semi-classical Schrödinger equation with vector potentials. Compared with the results in [21], our method achieves spectral accuracy in space by interpolating the Fourier series via the NonUniform Fast Fourier Transform (NUFFT) algorithm in the convection step. The NUFFT algorithm helps maintain high spatial accuracy of Fourier method, and at the same time improve the efficiency from $O(N^2)$ (of direct computation) to $O(N \log N)$ operations, where N is the total number of grid points. The kinetic step and potential step are solved by analytical solution with pseudo-spectral approximation, and, therefore, we obtain spectral accuracy in space for the whole method. We prove that the method is unconditionally stable, and we show improved error estimates for both the wave function and physical observables, which agree with the results in [3] for vanishing potential cases and are superior to those in [21]. Extensive one and two dimensional numerical studies are presented to verify the properties of the proposed method, and simulations of 3D problems are demonstrated to show its potential for future practical applications.

Keywords: semi-classical Schrödinger equation, vector potential, semi-Lagrangian time splitting method, nonuniform FFT

1. Introduction

Quantum effects play a significant role in many scientific and engineering areas, such as theoretical chemistry, solid-state mechanics and quantum optics, and the mathematical analysis and numerical simulation of Schrödinger equations are of fundamental importance. This type of equations form a canonical class of dispersive PDEs, i.e., equations where waves of different wavelengths propagate at different phase velocities. Whenever the magnetic field is considered, we need to incorporate the vector potentials in the Schrödinger equation.

In this paper, we consider the semi-classical Schrödinger equation with vector potentials, which has the form

$$i\varepsilon\partial_t u^\varepsilon = \frac{1}{2} (-i\varepsilon\nabla_x - \mathbf{A}(x))^2 u^\varepsilon + V(x)u^\varepsilon, \quad t \in \mathbb{R}^+, \quad x \in \mathbb{R}^3, \quad (1.1)$$

$$u^\varepsilon(x, 0) = u_0(x), \quad x \in \mathbb{R}^3, \quad (1.2)$$

where $u^\varepsilon(x, t)$ is the complex-valued wave function, $V(x) \in \mathbb{R}$ is the scalar potential and $\mathbf{A}(x) \in \mathbb{R}^3$ is the vector potential. The scalar potential and the vector potential are introduced to mathematically describe

*Corresponding author.

Email addresses: mayuyu@sjtu.edu.cn (Zheng MA), yong.zhang@univ-rennes1.fr (Yong ZHANG), zhennan@math.duke.edu (Zhennan ZHOU)

the electromagnetic field, i.e., the electric field $\mathbf{E}(x) \in \mathbb{R}^3$ and the magnetic field $\mathbf{B}(x) \in \mathbb{R}^3$ given as follows

$$\mathbf{E} = -\nabla V(x), \quad \mathbf{B} = \nabla \times \mathbf{A}(x). \quad (1.3)$$

The Schrödinger equation (1.1) above can be derived from the equation in the absence of the vector potential by local gauge transformation (see [29]). The quantum dynamics in the presence of the external electromagnetic field results in many far-reaching consequences in quantum mechanics, such as Landau levels, Zeeman effect and superconductivity. In the aspect of analysis, the Hamiltonian has different features in spectral and scattering properties (see [1]). Numerically, it gives new challenges as well, especially in the semi-classical regime. The presence of the vector potential introduces a convection term in the Schrödinger equation and in the meanwhile effectively modifies the scalar potential (see [21]).

In fact, one can simplify the potential description by imposing one more condition, namely, specifying the gauge. The electric field $\mathbf{E}(x) \in \mathbb{R}^3$ and magnetic field $\mathbf{B}(x) \in \mathbb{R}^3$ stay invariant in different gauges. One natural choice is, $\nabla_x \cdot \mathbf{A} = 0$, which is the so-called Coulomb gauge. In this gauge, the vector potential and the canonical momentum operator commute, $[\mathbf{A}, -i\varepsilon\nabla_x] = 0$, so that the modified “kinetic” part of the Schrödinger equation (1.1) can be simplified as follows

$$\frac{1}{2}(-i\varepsilon\nabla_x - \mathbf{A})^2 u^\varepsilon = -\frac{\varepsilon^2}{2}\Delta_x u^\varepsilon + i\varepsilon\mathbf{A} \cdot \nabla_x u^\varepsilon + \frac{1}{2}|\mathbf{A}|^2 u^\varepsilon. \quad (1.4)$$

In the Schrödinger equation, the wave function acts as an auxiliary quantity used to compute macroscopic physical quantities (physical observables) such as the position density

$$n(x, t) = |u^\varepsilon(x, t)|^2, \quad (1.5)$$

and the modified current density

$$\mathbf{J}(x, t) = \frac{1}{2}(\overline{u^\varepsilon}(-i\varepsilon\nabla_x - \mathbf{A})u^\varepsilon - u^\varepsilon(-i\varepsilon\nabla_x - \mathbf{A})\overline{u^\varepsilon}), \quad (1.6)$$

where \bar{f} denotes the complex conjugate of f . Actually, we have the following mass conservation equation

$$\frac{\partial}{\partial t}n + \nabla_x \cdot \mathbf{J} = 0. \quad (1.7)$$

We remark that n and \mathbf{J} are gauge invariant quantities. Another two important physical quantities are the *mass*

$$m(t) := \|u^\varepsilon(x, t)\|_{L^2}^2 = \int_{\mathbb{R}^3} n(t, x) dx, \quad (1.8)$$

and *the energy*

$$\mathcal{E}(t) := \frac{1}{2}\|(-i\varepsilon\nabla - \mathbf{A})u^\varepsilon\|_{L^2}^2 + \langle u^\varepsilon, V u^\varepsilon \rangle, \quad (1.9)$$

where $\langle f, g \rangle \equiv \int_{\mathbb{R}^d} f(x)\overline{g(x)} dx$ is the standard inner product. For $u^\varepsilon \in C(\mathbb{R}_t; L^2(\mathbb{R}^d) \cap \mathcal{S}(\mathbb{R}^d))$, these quantities are conserved through dynamics. We refer the readers to appendixes for detailed proofs.

In the semi-classical regime, namely $\varepsilon \ll 1$, the wave function u^ε is highly oscillatory both in space and time on the scale $O(\varepsilon)$, therefore it does not converge in the strong sense as $\varepsilon \rightarrow 0$. When $\varepsilon \ll 1$, several approximate methods other than directly solving the Schrödinger equation have been proposed, such as the level set method and the moment closure method based on the WKB analysis and the Wigner transform, see, for example, [9, 18, 16, 17]. The Gaussian beam method (or the Gaussian wave packet approach) is another important one, which allows accurate computation around caustics and captures phase information (see, for example, [14, 23, 25, 19]) with $O(\varepsilon^{1/2})$ model error. To improve the approximation accuracy, higher order Gaussian beam methods were introduced with an error $C_k(T)\varepsilon^{k/2}$ (see [31, 20]). However, it has been shown in [22, 33] that, for fixed ε , higher order Gaussian beam methods may not be a practical way to reduce the error. Whereas, the Hagedorn wave packets, studied by Hagedorn [13], analyzed and implemented as a

computational tool in [13, 11, 33], can effectively reduce the error for all $\varepsilon \in (0, 1]$. In [33], Zhou has extended this method to the vector potential case and provided a rigorous proof for the higher order convergence with the Galerkin approximation. Recently, Russo and Smereka in [26, 27] proposed a new approach based on the so-called Gaussian Wave packet transform, which is another worthy alternative.

Numerically, if one wants to directly simulate the Schrödinger equation (1.1), the oscillatory nature of the wave function gives rise to significant computational burdens. The computation of physical observables, like $n(x, t)$ and $\mathbf{J}(x, t)$, faces the same challenges. To our best knowledge, one of the best methods is the time splitting spectral method, introduced by Bao, Jin and Markowich in [3, 4, 17], where the meshing strategy $\Delta t = O(\varepsilon)$ and $\Delta x = O(\varepsilon)$ is sufficient to guarantee an accurate approximation of the wave function. To compute correct physical observables, the time step can be relaxed to $O(1)$.

Due to the presence of the vector potential, compared with the classical case, there are two major changes in (1.4): a modified scalar potential and a new convection term. In order to design an unconditional stable scheme, a semi-Lagrangian time splitting method was introduced by Jin and Zhou [21], where the meshing strategy $\Delta t = O(\varepsilon)$ and $\Delta x = O(\varepsilon)$ is sufficient to guarantee an accurate approximation of the wave function. Similarly, one can use ε independent time steps to capture correct physical observables. In the convection step, a polynomial interpolation technique was analyzed and implemented in [21], where the spatial accuracy was sacrificed for efficiency consideration. In fact, a spectral interpolation can be applied instead to improve spatial accuracy, unfortunately, it would increase the computational complexity from $O(N)$ (polynomial interpolation) to $O(N^2)$ (direct Fourier series summation), where N is the number of grid points. The primary issue is that the standard inverse FFT no longer applies since the evaluation points are not necessarily uniformly spaced. Hence, a balance between efficiency and accuracy is desired for the semi-Lagrangian method.

Thanks to the nonuniform Fast Fourier transform (NUFFT), (see, for example, [8, 12]), the problem can be solved ideally. This is the major motivation of our work. The nonuniform Fourier transform arises in a variety of application areas, from medical imaging to radio astronomy to the numerical solution of partial differential equations. When the sampling is uniform and the Fourier transform is desired at equispaced frequencies, the classical fast Fourier transform (FFT) has played a fundamental role in computation which requires only $O(N \log N)$ operations to compute N Fourier modes from N points rather than $O(N^2)$ operations. However, when the data is not sampled on an evenly partitioned mesh in either the “physical” or “frequency” domain, unfortunately, the FFT does not apply. Over the last few years, a number of algorithms have been developed to overcome this limitation and are often referred to as nonuniform FFT’s (NUFFT’s).

In this paper, we incorporate the NUFFT algorithm into the time splitting semi-Lagrangian method, and the computational complexity is $O(N \log N)$. The new method is proved to be unconditionally stable. Unlike the polynomial case, where special care is needed for the interpolation stencil, the interpolation is now done by a global spectral approximation. When time and space oscillations are resolved, namely, $\Delta x = O(\varepsilon)$ and $\Delta t = O(\varepsilon)$, we prove that our method is spectrally accurate in space and first order accurate in time. We also showed, in the framework of Wigner transform, that ε -independent time steps are allowed to compute the correct physical observables.

Extensive numerical experiments were carried out to validate our methods. The temporal error can easily be improved with a high order splitting scheme. In practice, the Strang splitting was applied in our simulation. In the one dimensional case, we have verified that the method converges spectrally in space and second order in time. We also show that when computing the physical observables, there is no need to resolve the time oscillations. Numerical experiments in two and three dimensions are presented.

The rest of the paper is organized in the following way. In Section 2, we present a detailed construction of the numerical method as well as a brief review of the NUFFT algorithm. Rigorous stability analysis and error estimates of the wave function are provided in Section 3, where we also analyzed the meshing strategy when computing the physical observables only. In section 4, we present various numerical tests to verify the properties of our method. We conclude in the last section with some comments and future directions.

2. Numerical methods

2.1. The time splitting and the spectral approximation

In this section, we shall adapt the time splitting spectral method introduced in [3, 21]. For simplicity, we focus on the one dimensional problem with periodic boundary condition. The extension to multidimensional cases is straightforward by tensor product. Here, we only present a first order time splitting scheme and the extension to higher order scheme has been described in [21]. The computational domain $[a, b]$ is discretized uniformly as $x_j = a + j\Delta x$, $j = 0, \dots, N - 1$, where $\Delta x = (b - a)/N$ and N is an even positive integer. Choose a constant time step Δt , and denote $t_n = n\Delta t$, $U^n = (U_0^n, \dots, U_{N-1}^n)^T$ with components U_j^n being the numerical approximation of $u^\varepsilon(x_j, t_n)$, and V_j as numerical approximation of $V(x_j)$.

We consider the one dimensional Schrödinger equation, which is reminiscent of equation (1.1) with the Coulomb gauge,

$$i\varepsilon\partial_t u^\varepsilon = -\frac{\varepsilon^2}{2}\Delta u^\varepsilon + i\varepsilon\mathbf{A} \cdot \nabla u^\varepsilon + \frac{1}{2}|\mathbf{A}|^2 u^\varepsilon + V u^\varepsilon, \quad a < x < b, \quad t > 0, \quad (2.10)$$

with periodic boundary conditions

$$u^\varepsilon(a, t) = u^\varepsilon(b, t), \quad u_x^\varepsilon(a, t) = u_x^\varepsilon(b, t), \quad (2.11)$$

and the initial value

$$u^\varepsilon(x, 0) = u_0^\varepsilon(x). \quad (2.12)$$

Note that, in one dimensional cases, \mathbf{A} is a scalar function and the potential gauge is not a well defined concept, but the numerical methods designed for equation (2.10) can naturally be extended to the multidimensional cases. In the framework of the time splitting method, to evolve (2.10) from t_n to t_{n+1} , we can first solve the Schrödinger equation with the kinetic part only

$$i\varepsilon\partial_t u^\varepsilon = -\frac{\varepsilon^2}{2}\Delta u^\varepsilon, \quad t \in [t_n, t_{n+1}], \quad (2.13)$$

then solve the potential equation

$$i\varepsilon\partial_t u^\varepsilon = \frac{1}{2}|\mathbf{A}|^2 u^\varepsilon + V u^\varepsilon, \quad t \in [t_n, t_{n+1}], \quad (2.14)$$

and finally solve the convection equation

$$\partial_t u^\varepsilon = \mathbf{A} \cdot \nabla u^\varepsilon, \quad t \in [t_n, t_{n+1}]. \quad (2.15)$$

To solve the above equations numerically, we first introduce a function space S_N as follows

$$S_N = \text{span}\{e^{i\mu_k(x-a)}, \mu_k = (2\pi k)/(b-a) \quad k = -N/2, \dots, N/2 - 1\}. \quad (2.16)$$

Let $\Pi_N : S_p := \{u(x) | u \in C^1([a, b]), u(a) = u(b), u'(a) = u'(b)\} \rightarrow S_N$ be the standard projection operator[28], i.e.,

$$(\Pi_N u)(x) = \sum_{k=-N/2}^{N/2-1} \tilde{u}_k e^{i\mu_k(x-a)}, \quad x \in [a, b], \quad \forall u(x) \in S_p, \quad (2.17)$$

with

$$\tilde{u}_k = \frac{1}{b-a} \int_a^b u(x) e^{-i\mu_k(x-a)} dx, \quad k = -N/2, \dots, N/2 - 1. \quad (2.18)$$

To compute the Fourier coefficient \tilde{u}_k , we approximate the integral in (2.18) by a numerical quadrature, i.e., the trapezoidal rule, on the uniform grid points, and the resulting summation is implemented with FFT efficiently. Equivalently, this numerical approximation allows us to define an interpolation of $u(x)$ on the grid points as follows

$$u_I(x) = \sum_{k=-N/2}^{N/2-1} \hat{u}_k e^{i\mu_k(x-a)}, \quad x \in [a, b], \quad (2.19)$$

with

$$\hat{u}_k = \frac{1}{N} \sum_{j=0}^{N-1} U_j e^{-i\mu_k(x_j-a)} = \frac{1}{N} \sum_{j=0}^{N-1} U_j e^{-i\frac{2\pi j k}{N}}, \quad k = -N/2, \dots, N/2-1. \quad (2.20)$$

Numerically, we can solve the free Schrödinger equation (2.13) analytically in the Fourier space

$$U_j^* = \sum_{k=-N/2}^{N/2-1} e^{-i\frac{\Delta t}{2}\varepsilon\mu_k^2} \hat{u}_k^n e^{i\mu_k(x_j-a)}, \quad (2.21)$$

and the potential step is integrated exactly in physical space

$$U_j^{**} = e^{-i(\frac{1}{2}|\mathbf{A}|^2 u_j^* + V_j)\Delta t/\varepsilon} U_j^*. \quad (2.22)$$

Generally speaking, for arbitrary vector potential $\mathbf{A}(x)$, it is not possible to solve the convection equation (2.15) analytically. Although many numerical methods are available for this equation, most of the prevailing ones have the CFL constraints which prevent large time steps compared with spatial mesh sizes. However, to capture accurate physical observables by solving the oscillatory wave function with unresolved time steps, it is necessary to apply an unconditionally stable method.

To solve the convection step numerically with improved stability condition, a semi-Lagrangian method with polynomial interpolations has been proposed in [21]. The semi-Lagrangian method consists of back-tracing along the characteristic and interpolation. To be precise, we solve the convection equation with periodic boundary conditions

$$\partial_t u^\varepsilon - \mathbf{A} \cdot \nabla u^\varepsilon = 0, \quad t \in [t_n, t_{n+1}]. \quad (2.23)$$

The corresponding characteristic line equation reads as

$$\frac{dx(t)}{dt} = -\mathbf{A}(x(t)), \quad x(t_{n+1}) = x_j. \quad (2.24)$$

We name the solution $x(t_n) = x_j^0$, which is obtained numerically by solving the ODE (2.24), as shifted target points hereafter. Along the characteristic line, we have $u^\varepsilon(x_j, t_{n+1}) = u^\varepsilon(x_j^0, t_n)$. However, since the shifted target points are not necessarily grid points, an interpolation is needed to approximate $u^\varepsilon(x_j^0, t_n)$. We can employ either global spectral interpolation, e.g., Fourier pseudo-spectral interpolation, or local polynomial interpolation, e.g., M -th order Lagrange polynomial interpolation [21].

When local polynomial interpolation applies, for each shifted target point x_j^0 , one needs to construct a polynomial interpolant from its adjacent grid points. Take the M -th order Lagrange polynomial interpolation for example, for each x_j^0 , one chooses M adjacent grid points to construct Lagrange polynomial interpolant with $O(\Delta x^M)$ errors. The total cost of the local polynomial interpolation is $O(N)$ for each step.

While in the global spectral interpolation, we first construct a spectral interpolation on grid points, and then evaluate the interpolation function at shifted target points. For the Fourier spectral interpolation, all the Fourier coefficients are computed within $O(N \log N)$ arithmetic operation with FFT. It is worthwhile to point out that FFT does not apply in evaluations simply because $\{x_j^0\}$ are not necessarily the uniformly distributed grid points. Direct evaluation of the finite Fourier series for each target point x_j^0 requires N

operations. Therefore, the total evaluation process cost is $O(N^2)$ and it is quite time consuming, especially in higher dimensions.

Compared with local polynomial interpolation, the Fourier interpolation is spectrally accurate in space but is bottlenecked in efficiency. With the NUFFT algorithm [12], we can improve the efficiency from $O(N^2)$ to $O(N \log N)$ without sacrificing its spectral accuracy. Note that the NUFFT is simply a fast algorithm for computing a discrete Fourier summation as encountered here. We would like to first present the semi-Lagrangian method with NUFFT before giving a brief review.

We conclude this section with the following remarks. When the vector potential \mathbf{A} is time independent, the backward characteristic tracing step is also independent of time. In other words, one just needs to solve (2.24) for the set of shifted target point $\{x_j^0\}$ once with sufficiently small time step, and use them for all future time steps. This step can be done in a preprocessed step with great precision. When the vector potential is time dependent, i.e., $\mathbf{A}(x, t)$, the backward characteristic tracing step needs to be done for every time step with $O(N)$ operations. And still, the choice of the time step for backward tracing is independent of ε or the time step for the whole method.

2.2. A semi-Lagrangian method for the convection step with NUFFT

To solve the convection equation (2.15) with the semi-Lagrangian method, as shown in previous sections, we are now faced with the following evaluation

$$U_j^{n+1} = u^\varepsilon(x_j^0, t_n) \approx \sum_{k=-N/2}^{N/2-1} \hat{u}_k^n e^{i\mu_k(x_j^0 - a)} = \sum_{k=-N/2}^{N/2-1} \hat{u}_k^n e^{ik \frac{2\pi(x_j^0 - a)}{b-a}}. \quad (2.25)$$

In general, the shifted target points x_j^0 are not necessarily uniformly distributed, therefore FFT does not apply to the Fourier series summation (2.25) due to the loss of algebraic structure of the transform matrix. The direct summation, which requires $O(N^2)$ arithmetic operations, will bottleneck the efficiency, especially for 2D and 3D problems. With the NUFFT algorithm, the evaluation (2.25) can be done within $O(N \log N)$ operations. Compared with the $O(N^2)$ complexity, the efficiency improvement to $O(N \log N)$ is quite spectacular. We then incorporate the NUFFT algorithm to the semi-Lagrangian method, and details of the improved method are given as follows

Algorithm 1 The semi-Lagrangian method with NUFFT

1. Backward tracing to find the shifted target points x_j^0 .
 2. Compute the Fourier spectral interpolation of $u^\varepsilon(x, t_n)$ using grid points x_j with FFT.
 3. Evaluate $U_j^{n+1} = u^\varepsilon(x_j^0, t_{n+1})$ in (2.25) via NUFFT.
-

The total cost of **Algorithm 1** is composed of three parts. Step 1 can be solved by ODE solvers within $O(N)$ operations. The Fourier coefficients in Step 2 can be computed by forward FFT within $O(N \log N)$ operations. The evaluation in Steps 3 can be done within $O(N \log N + N)$ operations by NUFFT. In summary, the total cost is $O(N + N \log N)$. The spatial accuracy is improved from polynomial accuracy to spectral accuracy and numerical confirmation will be presented. Extensions to multi-dimensional cases are simple and straightforward.

2.3. A brief review of the NUFFT algorithm

In this section, we present a quite brief review of the NUFFT algorithm. The algorithm is aimed to accelerate Fourier series evaluation, which involves nonuniform points in the physical and/or Fourier domains, up to a complexity of $O(N \log N)$. There exist many versions, here we follow the discussion in [12], which describes a simple and fast implementation using Gaussian kernels for interpolation.

We define the nonuniform discrete Fourier transform of type 1 and 2 in one dimension as follows

$$\text{type 1 : } \quad F(k) = \sum_{j=0}^{N-1} f_j e^{-ikx_j}, \quad k = -M/2, \dots, M/2 - 1, \quad (2.26)$$

$$\text{type 2 : } \quad f(x_j) = \sum_{k=-M/2}^{M/2-1} F(k) e^{ikx_j}, \quad j = 0, 1, \dots, N, \quad (2.27)$$

where $x_j \in [0, 2\pi]$ are nonequispaced grid points and f_j are complex numbers.

For simplicity, to illustrate the basic underlying idea, we consider the one dimensional type 1 case. The type 2 summation, used in our semi-Lagrangian method, can be viewed as an inverse of type 1 and we refer the readers to [12] for details. Note that equation (2.26) describes the exact Fourier coefficients of the function

$$f(x) = \sum_{j=0}^{N-1} f_j \delta(x - x_j), \quad (2.28)$$

which is viewed as a periodic function on $[0, 2\pi]$. Here $\delta(x)$ is the Dirac delta function. By convolving with the 1D periodic heat kernel on $[0, 2\pi]$, i.e., $g_\tau(x) = \sum_{l=-\infty}^{\infty} e^{-(x-2l\pi)^2/4\tau}$, we can construct a 2π -periodic C^∞ function f_τ as follows

$$f_\tau(x) = f * g_\tau(x) = \int_0^{2\pi} f(y) g_\tau(x - y) dy. \quad (2.29)$$

In fact, f_τ is a good approximation of f and can be well-resolved by a uniform mesh in x . The Fourier coefficients $F_\tau(k) = \frac{1}{2\pi} \int_0^{2\pi} f_\tau(x) e^{-ikx} dx$ can be approximated with high accuracy using the standard FFT on an oversampled grid

$$F_\tau(k) \approx \frac{1}{M_r} \sum_{m=0}^{M_r-1} f_\tau(2\pi m/M_r) e^{-ik2\pi m/M_r}, \quad (2.30)$$

where

$$f_\tau(2\pi m/M_r) = \sum_{j=0}^{N-1} f_j g_\tau(2\pi m/M_r - y_j). \quad (2.31)$$

Once the values $F_\tau(k)$ are known, by convolution theorem, we have

$$F(k) = \sqrt{\frac{\pi}{\tau}} e^{k^2 \tau} F_\tau(k). \quad (2.32)$$

Optimal choice of related parameters involves a bit of analysis and we omit it here. Following the argument in [12], we choose $M_r = 2M$ and $\tau = 12/M^2$ and use a Gaussian to spread each source to its nearest 24 points, then it yields about 12 digits accuracy. For 6 digits accuracy, we choose $\tau = 6/M^2$ and spread each source to its nearest 12 points. In computation practice, we choose the 12-digit accuracy if not stated otherwise.

3. Numerical analysis

In this section, we shall study the stability, convergence of the wave function and physical observables.

3.1. Stability analysis

For any function $u(x) \in S_p$, let $\mathbf{U} = (u(x_0), \dots, u(x_{N-1}))^T$ be the grid vector of u . Define $\|\cdot\|_{l^2}$ as the discrete l^2 norm and $\|\cdot\|_{L^2}$ as L^2 norm for function in S_p as follows

$$\|\mathbf{U}\|_{l^2} = \left(\Delta x \sum_{j=0}^{N-1} |U_j|^2 \right)^{1/2}, \quad \|u\|_{L^2} = \left(\int_a^b |u(x)|^2 dx \right)^{1/2}. \quad (3.33)$$

After simple calculations, we have $\|u_I(x)\|_{L^2} = \|U\|_{l^2}$ for any $u \in S_p$.

LEMMA 3.1. *For every time step $t \in [t_n, t_{n+1}]$, after solving the kinetic step (2.13) and the potential step (2.14), we have*

$$\|\mathbf{U}^{**}\|_{l^2} = \|\mathbf{U}^n\|_{l^2}. \quad (3.34)$$

Proof. The proof is similar as that in [3] and we omit details here for brevity. \square

To solve the convection equation with semi-Lagrangian method, one first follows backwards along the characteristics. For the characteristics equation with arbitrary initial point $x_0 \in [a, b]$,

$$\frac{dx(t)}{dt} = -\mathbf{A}(x(t)), \quad x(t_0) = x_0, \quad x_0 \in [a, b]. \quad (3.35)$$

We can define a mapping $E(t, t_0)$ on S_p as follows

$$(E(t, t_0)v)(x_0) := v(x(t)), \quad v \in S_p. \quad (3.36)$$

Since (3.35) is an autonomous system, $E(t, t_0)$ is a function of $t - t_0$ only. For this reason, we will write $E(t - t_0)$ instead of $E(t, t_0)$. If errors coming from the backward tracing and the spectral interpolation are negligible, i.e., $u_I^{n+1}(x_j)$ is “exact”, the semi-Lagrangian method using NUFFT can be described as

$$u_I^{n+1}(x) = \Pi_N E(\Delta t) u_I^{**}(x), \quad (3.37)$$

where $u_I^{**}(x)$ is the spectral interpolant of $u^{**}(x)$.

LEMMA 3.2. *Assume $\mathbf{A} \in C^1([a, b])$ and is divergence free, i.e., $\nabla \cdot \mathbf{A} = 0$, the semi-Lagrangian scheme (3.37) is unconditionally stable and we have*

$$\|u_I^{n+1}\|_{L^2} \leq \|u_I^{**}\|_{L^2}. \quad (3.38)$$

Proof. Starting from (3.37),

$$\|u_I^{n+1}\|_{L^2} = \|\Pi_N E(\Delta t) u_I^{**}\|_{L^2} \leq \|E(\Delta t) u_I^{**}\|_{L^2}, \quad (3.39)$$

Since \mathbf{A} is divergence free, we have $\|E(\Delta t)\|_{(L^2)^*} \leq 1$ and $\|u_I^{n+1}\|_{L^2} \leq \|u_I^{**}\|_{L^2}$. \square

Remark 3.1. *The Lemma can also be easily extended to more general \mathbf{A} . We refer to [30] for more discussions.*

Combing Lemma (3.1) and (3.2), we obtain the stability result as follows

THEOREM 3.1. *The semi-Lagrangian time splitting scheme with NUFFT method, (2.21), (2.22) and (2.25), is unconditionally stable. In fact, with any mesh size and time step*

$$\|\mathbf{U}^{n+1}\|_{l^2} \leq \|\mathbf{U}^n\|_{l^2}, \quad n = 1, 2, \dots \quad (3.40)$$

Proof. According to Lemma (3.1), $\|\mathbf{U}^{**}\|_{l^2} = \|\mathbf{U}^n\|_{l^2}$. Following Lemma (3.2), we have

$$\|\mathbf{U}^{n+1}\|_{l^2} = \|u_I^{n+1}\|_{L^2} \leq \|u_I^{**}\|_{L^2} = \|\mathbf{U}^{**}\|_{l^2} = \|\mathbf{U}^n\|_{l^2}.$$

\square

3.2. Error estimates of the wave function

In this section, we study the numerical approximation error of the wave function and the meshing strategy. We assume that the wave function is ε -oscillatory in both space and time. More specifically, there exist positive constants B_m, C_m, D_m , which are independent of t, x and ε , such that

$$\left\| \frac{\partial^{m_1+m_2}}{\partial x^{m_1} \partial t^{m_2}} u(x, t) \right\|_{C([0, T]; L^2)} \leq \frac{1}{\varepsilon^{m_1+m_2}} C_{m_1+m_2}, \quad m = m_1 + m_2, \quad m_1, m_2 \in \mathbb{N}^+, \quad (3.41)$$

$$\left\| \frac{\partial^m}{\partial x^m} \mathbf{A}(x) \right\|_{L^2} \leq D_m, \quad \left\| \frac{\partial^m}{\partial x^m} V(x) \right\|_{L^2} \leq B_m. \quad (3.42)$$

Note that in (3.41), the differentiation operator is unbounded for general smooth functions, but it is bounded in the subspace of smooth L^2 function which are at most ε -oscillatory. The assumptions (3.42) imply that the potentials are smooth with ε independent bounds. We use f_I to denote the spectral approximation based on the discrete data $f(x_j)$ as mentioned in the previous section. Now we can prove the following error estimate for the first order semi-Lagrangian time splitting method (abbreviated by SL-TS) using NUFFT.

The proof basically follows Theorem 4 in [21] and also Theorem 4.1 in [3], but it differs from the previous versions because it shows spectral accuracy in space in the presence of vector potentials.

THEOREM 3.2. *Let $u^\varepsilon(x, t)$ be the exact solution to equation (2.10), $u^{\varepsilon, n}$ be the discrete approximation by the first order SL-TS method. We assume the characteristic equations (2.24) are numerically solved with negligible small error, and the NUFFT is used in the semi-Lagrangian method for the convection step also with negligible small error. Under assumptions (3.41)-(3.42), we further assume $\Delta x = O(\varepsilon)$ and $\Delta t = O(\varepsilon)$, then for any time $t \in [0, T]$, we have*

$$\|u^\varepsilon(t_n) - u_I^{\varepsilon, n}\|_{L^2} \leq G_m \frac{T}{\Delta t} \left(\frac{\Delta x}{\varepsilon} \right)^m + \frac{CT\Delta t}{\varepsilon}, \quad (3.43)$$

where $m \in \mathbb{N}^+$ is the regularity index of $u^\varepsilon(x, t)$, C is a positive constant independent of $\Delta t, \Delta x, \varepsilon, m$, and G_m is a positive constant independent of $\Delta t, \Delta x$ and ε .

Proof. In the proof, the constants involved are assumed to be independent of ε if not stated clearly. For clarity, we rewrite the equation (2.10) as

$$\partial_t u^\varepsilon = (\mathcal{A} + \mathcal{B} + \mathcal{C}) u^\varepsilon, \quad (3.44)$$

where

$$\mathcal{A} = \frac{i\varepsilon}{2} \Delta, \quad \mathcal{B} = -\frac{i}{\varepsilon} \left(\frac{1}{2} |\mathbf{A}|^2 + V \right), \quad \mathcal{C} = \mathbf{A} \cdot \nabla.$$

Let $u^\varepsilon(t_n)$ be the exact solution at $t = t_n$, then

$$u^\varepsilon(t_{n+1}) = e^{(\mathcal{A} + \mathcal{B} + \mathcal{C})\Delta t} u^\varepsilon(t_n). \quad (3.45)$$

Define the solution obtained by the (first order) operator splitting (without spatial discretization) as

$$w^{n+1} = e^{\mathcal{C}\Delta t} e^{\mathcal{B}\Delta t} e^{\mathcal{A}\Delta t} u^\varepsilon(t_n). \quad (3.46)$$

Note that w^{n+1} differs from $u^\varepsilon(t_{n+1})$ due to the operator splitting error. As shown in [21], the local splitting error is

$$\|u^\varepsilon(t_{n+1}) - w^{n+1}\|_{L^2} = O\left(\frac{\Delta t^2}{\varepsilon}\right). \quad (3.47)$$

By triangle inequality, we have

$$\|u^\varepsilon(t_{n+1}) - u_I^{\varepsilon, n+1}\|_{L^2} \leq \|u^\varepsilon(t_{n+1}) - w^{n+1}\|_{L^2} + \|w^{n+1} - w_I^{n+1}\|_{L^2} + \|w_I^{n+1} - u_I^{\varepsilon, n+1}\|_{L^2}, \quad (3.48)$$

where w_I^{n+1} is the spectral interpolation approximation of w^{n+1} . The first term of (3.48) is the splitting error (3.47), the second term gives the spectral approximation error and it is bounded by $C_m(\frac{\Delta x}{\varepsilon})^m$. Up to this point, the analysis agrees with the previous results. But, we need to analyze the last term, which is the one-step error term introduced by numerical approximations. Especially, since spectral approximation is utilized in the convection step, the resulting error is different from the one in [21], and hence needs to be carefully investigated.

In the SL-TS method, the potential step governed by operator \mathcal{B} is solved analytically, while the kinetic step and convection step governed by operators \mathcal{A} and \mathcal{C} are evolved by numerical approximations, denoted by \mathcal{A}_{SP} and \mathcal{C}_{SL} respectively. By triangle inequality:

$$\begin{aligned} \|w_I^{n+1} - u_I^{\varepsilon, n+1}\|_{L^2} &= \|w^{n+1} - u^{\varepsilon, n+1}\|_{L^2} \\ &= \|e^{\mathcal{C}\Delta t} e^{\mathcal{B}\Delta t} e^{\mathcal{A}\Delta t} u^\varepsilon(t_n) - e^{\mathcal{C}_{SL}\Delta t} e^{\mathcal{B}\Delta t} e^{\mathcal{A}_{SP}\Delta t} u^{\varepsilon, n}\|_{L^2} \\ &\leq \|e^{\mathcal{C}\Delta t} e^{\mathcal{B}\Delta t} e^{\mathcal{A}\Delta t} u^\varepsilon(t_n) - e^{\mathcal{C}\Delta t} e^{\mathcal{B}\Delta t} e^{\mathcal{A}_{SP}\Delta t} u^\varepsilon(t_n)\|_{L^2} \\ &\quad + \|e^{\mathcal{C}\Delta t} e^{\mathcal{B}\Delta t} e^{\mathcal{A}_{SP}\Delta t} u^\varepsilon(t_n) - e^{\mathcal{C}_{SL}\Delta t} e^{\mathcal{B}\Delta t} e^{\mathcal{A}_{SP}\Delta t} u^\varepsilon(t_n)\|_{L^2} \\ &\quad + \|e^{\mathcal{C}_{SL}\Delta t} e^{\mathcal{B}\Delta t} e^{\mathcal{A}_{SP}\Delta t} u^\varepsilon(t_n) - e^{\mathcal{C}_{SL}\Delta t} e^{\mathcal{B}\Delta t} e^{\mathcal{A}_{SP}\Delta t} u^{\varepsilon, n}\|_{L^2}. \end{aligned} \quad (3.49)$$

The first term on the right hand side of (3.49) measures the spectral approximation accuracy of $u^\varepsilon(t_n)$ in the kinetic step, so as is analyzed in [3, 21], this term is of order $O((\frac{\Delta x}{\varepsilon})^m)$ for any positive integer m .

The second term in (3.49) measures the numerical approximation accuracy of $e^{\mathcal{B}\Delta t} e^{\mathcal{A}_{SP}\Delta t} u^\varepsilon(t_n)$ in the convection step. We observe that, by stability analysis in the kinetic step and the potential,

$$\|e^{\mathcal{B}\Delta t} e^{\mathcal{A}_{SP}\Delta t} u^\varepsilon(t_n)\|_{L^2} = \|u^\varepsilon(t_n)\|_{L^2}.$$

Then, the local error analysis in Section 2 implies that, when the errors in computing the shifted grid points and NUFFT are minimal, the second term is of order $O((\frac{\Delta x}{\varepsilon})^m)$ for any positive integer m , which is dominated by the spectral interpolation error.

The last term in (3.49) links the numerical error of the numerical solutions between two consecutive time steps, where numerical stability is crucial. It can also easily be shown that the operator $e^{\mathcal{A}\Delta t}$, $e^{\mathcal{B}\Delta t}$ and $e^{\mathcal{C}\Delta t}$ (in the Coulomb gauge) are unitary operators with respect to periodic smooth functions in the L^2 norm, which implies $\|e^{\mathcal{A}\Delta t}\|_{L^2} = \|e^{\mathcal{B}\Delta t}\|_{L^2} = \|e^{\mathcal{C}\Delta t}\|_{L^2} = 1$. By stability analysis in the previous section, we have shown that

$$\|e^{\mathcal{A}_{SP}\Delta t}\|_{L^2} = 1 \quad \|e^{\mathcal{C}_{SL}\Delta t}\|_{L^2} \leq 1.$$

So, we conclude the following estimate for the last term of the right hand side of (3.49)

$$\begin{aligned} &\|e^{\mathcal{C}_{SL}\Delta t} e^{\mathcal{B}\Delta t} e^{\mathcal{A}_{SP}\Delta t} u^\varepsilon(t_n) - e^{\mathcal{C}_{SL}\Delta t} e^{\mathcal{B}\Delta t} e^{\mathcal{A}_{SP}\Delta t} u^{\varepsilon, n}\|_{L^2} \\ &\leq \|e^{\mathcal{C}_{SL}\Delta t}\|_{L^2} \|e^{\mathcal{B}\Delta t} e^{\mathcal{A}_{SP}\Delta t} u^\varepsilon(t_n) - e^{\mathcal{B}\Delta t} e^{\mathcal{A}_{SP}\Delta t} u^{\varepsilon, n}\|_{L^2} \\ &\leq \|e^{\mathcal{C}_{SL}\Delta t}\|_{L^2} \|u^\varepsilon(t_n) - u_I^{\varepsilon, n}\|_{L^2} \\ &\leq \|u^\varepsilon(t_n) - u_I^{\varepsilon, n}\|_{L^2}. \end{aligned} \quad (3.50)$$

This leads to

$$\|w_I^{n+1} - u_I^{\varepsilon, n+1}\|_{L^2} \leq \|u^\varepsilon(t_n) - u_I^{\varepsilon, n}\|_{L^2} + C'_m \left(\frac{\Delta x}{\varepsilon}\right)^m, \quad (3.51)$$

where C'_m is a constant, which is t, x, ε independent. So now we have a recursive relation

$$\|u^\varepsilon(t_{n+1}) - u_I^{\varepsilon, n+1}\|_{L^2} \leq \|u^\varepsilon(t_n) - u_I^{\varepsilon, n}\|_{L^2} + C_1 \left(\frac{\Delta x}{\varepsilon}\right)^m + C_2 \left(\frac{\Delta t^2}{\varepsilon}\right), \quad (3.52)$$

where C_1, C_2 are some constants, which are t, x, ε independent.

Based on the recursive relation for $\|u^\varepsilon(t_n) - u_I^{\varepsilon, n}\|_{L^2}$, by induction, one concludes that,

$$\|u^\varepsilon(t_n) - u_I^{\varepsilon, n}\|_{L^2} \leq G_m \frac{T}{\Delta t} \left(\frac{\Delta x}{\varepsilon}\right)^m + \frac{CT\Delta t}{\varepsilon}. \quad (3.53)$$

This completes the proof. \square

This theorem implies if $\delta > 0$ is the desired error bound in L^2 norm such that $\|u^\varepsilon(t_n) - u_I^{\varepsilon,n}\|_{L^2} < \delta$, the corresponding meshing strategy is

$$\frac{\Delta t}{\varepsilon} = O(\delta), \quad \frac{\Delta x}{\varepsilon} = O(\delta^{1/m} \Delta t^{1/m}), \quad (3.54)$$

where $m \geq 1$ is an arbitrary integer. For higher order operator splitting technique, similar analysis can be done, which is omitted in this paper.

We remark that, the meshing strategy (3.54) agrees with the results in [3] where only the vector potential is absent, and is obviously better than those in [21], because in that work polynomial interpolation is applied in the semi-Lagrangian method and thus the whole numerical scheme does not have spectral accuracy in space.

3.3. Errors estimates for the physical observables

In general, if one only cares about the physical observables, weaker conditions in the meshing strategy may be sufficient (see [3, 21]), where the Wigner transform can be used to illustrate this point. For $f, g \in L^2(\mathbb{R}^d)$, the Wigner transform is defined as a phase-space function

$$w^\varepsilon(f, g)(t, x, \xi) = \frac{1}{(2\pi)^d} \int_{\mathbb{R}^d} e^{iy \cdot \xi} \bar{f}(x - \frac{\varepsilon}{2}y) g(x + \frac{\varepsilon}{2}y) dy. \quad (3.55)$$

Denote $w^\varepsilon = w^\varepsilon(u^\varepsilon, u^\varepsilon)$, as $\varepsilon \rightarrow 0$, the Wigner transform converges to the Wigner measure $w^0 = \lim_{\varepsilon \rightarrow 0} w^\varepsilon(u^\varepsilon, u^\varepsilon)$, where the limit is defined in an appropriate weak sense.

Let $a(x, \xi)$ be a smooth real-valued phase space function with sufficient decay at infinity, called a semi-classical symbol. Then the self-adjoint pseudo-differential operator $A^\varepsilon := a(x, \varepsilon D)^W$ is called an observable, here $D = i\nabla_x$ and W stands for the Weyl quantization. Then the average of this observable in this state is defined as

$$E_a^\varepsilon(t) = \int_{\mathbb{R}^d} \bar{u}^\varepsilon(t, x) (a(x, \varepsilon D)^W u^\varepsilon(t, x)) dx. \quad (3.56)$$

An important property of the Wigner transform is the duality identity

$$\int_{\mathbb{R}^d} \bar{u}^\varepsilon(t, x) (a(x, \varepsilon D)^W u^\varepsilon(t, x)) dx = \int_{\mathbb{R}^d \times \mathbb{R}^d} w^\varepsilon(t, x, \xi) a(x, \xi) dx d\xi. \quad (3.57)$$

As a result, $E_a^\varepsilon(t)$ can be taken to the semi-classical limit via

$$\lim_{\varepsilon \rightarrow 0} E_a^\varepsilon(t) = \int_{\mathbb{R}^d \times \mathbb{R}^d} w^0(t, x, \xi) a(x, \xi) dx d\xi. \quad (3.58)$$

Let \tilde{w}^ε be the Wigner transform of the numerical approximation solution. One can easily prove the following inequality

$$\|E_a^\varepsilon - \tilde{E}_a^\varepsilon\| \leq \|a\|_{\mathcal{E}} \cdot \|w^\varepsilon - \tilde{w}^\varepsilon\|_{\mathcal{E}^*} \leq C \|a\|_{\mathcal{E}} \cdot \|u^\varepsilon - \tilde{u}^\varepsilon\|_{L^2(a,b)}, \quad (3.59)$$

for $a \in \mathcal{E}$, which is the following Banach space

$$\mathcal{E} = \left\{ \phi \in C_0(\mathbb{R}_x^d \times \mathbb{R}_\xi^d) : (\mathcal{F}_{\xi \rightarrow v} \phi) \in L^1(\mathbb{R}_v^d; C_0(\mathbb{R}_x^d)) \right\}.$$

\mathcal{F} denotes the Fourier transform and \mathcal{E}^* is the dual space of \mathcal{E} . We remark that, when the wave function is decaying sufficiently fast at infinity, the Banach space can be extended.

In each time step $t \in [t_n, t_{n+1}]$ after operator splitting, the error in the wave function is introduced due to the spectral approximation and NUFFT (which is minimal). By Theorem (3.2) and above inequality (3.59), the error in the corresponding Wigner transform can be estimated.

The estimate (3.59) implies that, the spatial meshing strategy $\Delta x/\varepsilon = O(\delta^{1/m}\Delta t^{1/m})$ is sufficient to guarantee an $O(\delta)$ error in all physical observables caused by spectral approximations on the time interval $[0, T]$.

The splitting error in computing the physical observables, as discussed in [21], is $O(\varepsilon)$ since the limit classical equation is ε -independent and the time splitting of the Schrödinger equation corresponds to the time splitting of the Wigner equation. In the kinetic step and the potential step, the time integrations are performed exactly. In the convection part, the backward characteristic tracing is done in a preprocessed step with sufficiently fine yet ε independent time steps. Therefore, there is no ε -dependent error at all in time discretizations.

After all these considerations, we conclude that the SL-TS using NUFFT, can be taken to capture correct physical observables. It means that with time step $\Delta t = O(\delta)$ and spatial meshing strategy $\Delta x = O(\varepsilon)$, one gets numerical solutions with $O(\delta)$ error in the Wigner transforms $\varepsilon \rightarrow 0$, and as a result, $O(\delta)$ error in all the physical observables.

4. Numerical examples

In this section, we shall confirm the accuracy and efficiency of the proposed method with extensive one dimensional numerical studies, and provide simulation examples in two and three dimensional cases. The reference solutions are obtained by the time-explicit spectral method (TESP) with fine mesh size and time step, especially the convection equation is solved by the standard fourth order Runge-Kutta method and the spatial derivative was approximated by the Fourier spectral method [21]. Errors in wave function are computed in l^2 norm, while errors of physical observables are measured by their cumulative function's l^2 norm.

Example 4.1. Time-dependent vector potential.

In this example, we take the same one-dimensional example in [21] with a time-dependent vector potential. The computation domain is $C = [0, 2\pi]$ and the final time is $T = 0.4$. The scalar potential is $V(x) = 1$ and the vector potential is $\mathbf{A}(x, t) = \sin(x - 2t)/10$. The initial value is $u_0(x) = e^{-10(x-\pi)^2} e^{i \cos(x)/\varepsilon}$.

Errors of wave function, position density and current density are defined as follows:

$$E_u = \|u_{\Delta t}^N - u^{\text{ref}}\|_{l^2}, \quad E_n = \|\tilde{n}_{\Delta t}^N - \tilde{n}^{\text{ref}}\|_{l^1}, \quad E_I = \|\tilde{I}_{\Delta t}^N - \tilde{I}^{\text{ref}}\|_{l^1}, \quad (4.60)$$

where $u_{\Delta t}^N$ is the numerical solution obtained with $\Delta x = \frac{2\pi}{N}$ and Δt , u^{ref} is the reference solution obtained by TESP with very fine mesh and time step, and \tilde{n}, \tilde{I} are the corresponding cumulative functions

$$\tilde{n}(x) = \int_0^x n(s)ds, \quad \tilde{I}(x) = \int_0^x I(s)ds, \quad 0 < x < 2\pi. \quad (4.61)$$

The current density is defined as $I(t, x) = \varepsilon \text{Im}(\bar{u}^\varepsilon(t, x) \nabla_x u^\varepsilon(t, x)) = \frac{\varepsilon}{2i} (\bar{u}^\varepsilon \nabla_x u^\varepsilon - u^\varepsilon \nabla_x \bar{u}^\varepsilon)$.

We show in Table (1) and Figure (1) that with sufficient fine time step $\Delta t = 10^{-6}\varepsilon$, when $\Delta x = O(\varepsilon)$, the errors in the wave function and in the physical observables decrease exponentially fast as the spatial grid points increase until they reach a minimal number, which is dominated by the error in the NUFFT algorithm. Therefore, if the error in NUFFT is negligible, we have confirmed that the proposed method achieves spectral accuracy in space.

For various ε , with correspondingly sufficiently fine spatial mesh size, $\Delta x = \frac{2\pi}{32}\varepsilon$, we show the convergence studies in time steps in Table (2), and the numerical errors are plotted in Figure (2). The plots obviously show that we have the second order convergence in Δt for both wave functions and physical observables. This agrees with the Strang splitting we have used in the time splitting. Also, from Table (2) we see that, even if $\Delta t \gg \Delta x$ and $\Delta t \gg \varepsilon$, the numerical method is still stable. This verifies the unconditional stability of the whole time splitting spectral method.

Another important observation to make is, by checking each column of Table (2), we learn that, for fixed Δt , as ε decreases, the error in the wave functions increases proportionally, while the error in the physical

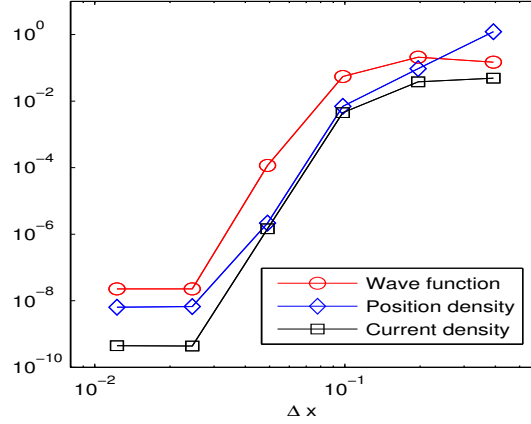


Figure 1: Log-log plot of errors of the wave function (l^2 norm), the position densities (l^1 norm), and current densities (l^1 norm) versus mesh sizes Δx for $\varepsilon = 1/32$ in Example 4.1.

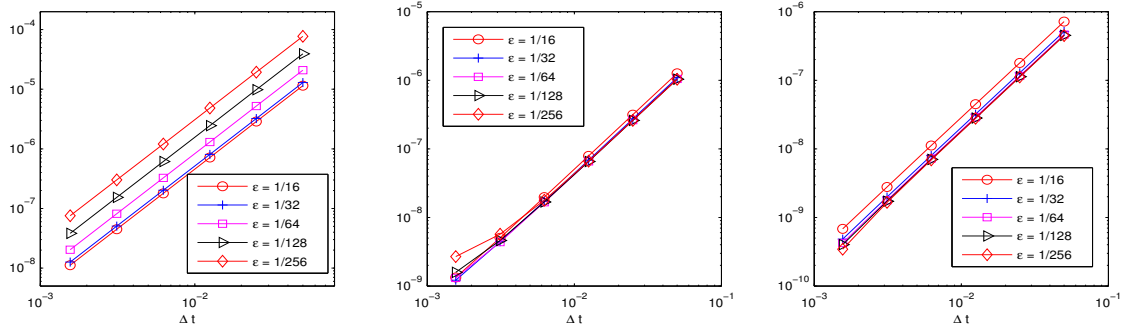


Figure 2: Log-log plot of the errors of the wave function (left), the position densities (middle), and current densities (right) versus time steps Δt for different ε in Example 4.1.

observables stay almost unchanged. Especially, we observe that (for example, in the first column of Table (2)), when $\Delta t \gg \Delta x$ and $\Delta t \gg \varepsilon$, the accuracy in the physical observables are pretty accurate. It justifies that we can take ε independent time steps to capture correct physical observables. The simulation time scales like $O(1/\varepsilon)$ if we only compute the physical observables, and it scales like $O(1/\varepsilon^2)$ if one needs to simulate the wave functions as well.

Table 1: Spatial errors computed with $\Delta x = \frac{2\pi}{N}$ and very fine time step $\Delta t = 10^{-6}\varepsilon$ for $\varepsilon = 1/32$ in Example 4.1. Reference solution is obtained by TESP with $\Delta x = \frac{2\pi}{4096}$ and $\Delta t = 10^{-6}\varepsilon$.

N	8	16	32	64	128	256
E_u	1.4844E-01	2.0897E-01	5.4851E-02	1.1685E-04	2.2790E-08	2.2602E-08
E_n	1.2187	9.3894E-02	6.9707E-03	2.1646E-06	6.6955E-09	6.3930E-09
E_I	4.8682E-02	3.8011E-02	4.5217E-03	1.4634E-06	4.3334E-10	4.4653E-10

Example 4.2. Simulation of a 2D system

In this example, we apply the new method to an essentially 2D model as is detailed in [21]. The vector potential is $\mathbf{A} = \frac{1}{2}(-\cos(y), \sin(x))^T$ and scalar potential vanishes, i.e., $V = 0$. The initial wave function is

Table 2: Temporal errors computed with $\Delta x = \frac{2\pi}{32}\varepsilon$ and different time steps $\Delta t_j = \frac{1}{10 \times 2^j}, j = 1, \dots, 6$ in Example 4.1. Reference solution is obtained by TESP with $\Delta x = \frac{2\pi}{32}\varepsilon$ and $\Delta t = 10^{-6}\varepsilon$.

E_u	Δt_1	Δt_2	Δt_3	Δt_4	Δt_5	Δt_6
$\varepsilon = \frac{1}{16}$	1.1461E-05	2.8641E-06	7.1595E-07	1.7898E-07	4.4740E-08	1.1181E-08
$\varepsilon = \frac{1}{32}$	1.2923E-05	3.2295E-06	8.0728E-07	2.0181E-07	5.0446E-08	1.2606E-08
$\varepsilon = \frac{1}{64}$	2.0866E-05	5.2144E-06	1.3034E-06	3.2585E-07	8.1458E-08	2.0361E-08
$\varepsilon = \frac{1}{128}$	3.9232E-05	9.8038E-06	2.4507E-06	6.1266E-07	1.5316E-07	3.8293E-08
$\varepsilon = \frac{1}{256}$	7.7212E-05	1.9295E-05	4.8231E-06	1.2057E-06	3.0140E-07	7.5325E-08
E_n	Δt_1	Δt_2	Δt_3	Δt_4	Δt_5	Δt_6
$\varepsilon = \frac{1}{16}$	1.2604E-06	3.1537E-07	7.8930E-08	1.9808E-08	5.0278E-09	1.3343E-09
$\varepsilon = \frac{1}{32}$	1.0910E-06	2.7306E-07	6.8388E-08	1.7209E-08	4.4144E-09	1.2172E-09
$\varepsilon = \frac{1}{64}$	1.0466E-06	2.6205E-07	6.5737E-08	1.6647E-08	4.3745E-09	1.3086E-09
$\varepsilon = \frac{1}{128}$	1.0356E-06	2.5952E-07	6.5318E-08	1.6756E-08	4.6157E-09	1.5836E-09
$\varepsilon = \frac{1}{256}$	1.0338E-06	2.5990E-07	6.6230E-08	1.7801E-08	5.6972E-09	2.6858E-09
E_I	Δt_1	Δt_2	Δt_3	Δt_4	Δt_5	Δt_6
$\varepsilon = \frac{1}{16}$	7.1615E-07	1.7901E-07	4.4738E-08	1.1171E-08	2.7788E-09	6.8085E-10
$\varepsilon = \frac{1}{32}$	5.1362E-07	1.2839E-07	3.2084E-08	8.0066E-09	1.9871E-09	4.8226E-10
$\varepsilon = \frac{1}{64}$	4.6330E-07	1.1581E-07	2.8932E-08	7.2115E-09	1.7815E-09	4.2398E-10
$\varepsilon = \frac{1}{128}$	4.5076E-07	1.1267E-07	2.8138E-08	7.0051E-09	1.7219E-09	4.0109E-10
$\varepsilon = \frac{1}{256}$	4.4759E-07	1.1183E-07	2.7889E-08	6.9018E-09	1.6551E-09	3.4344E-10

localized at $(x_0, y_0) = (0.1, -0.02)$ with $O(\varepsilon)$ oscillation,

$$u_0(x, y) = e^{-20(x-x_0)^2 - 20(y-y_0)^2} e^{i \sin(x) \sin(y)/\varepsilon}. \quad (4.62)$$

The computation domain is chosen as $[-\pi, \pi] \times [-\pi, \pi]$. Here, we numerically compute the density evolution for different $\varepsilon = 1/16, 1/32, 1/64, 1/128$ with mesh size $h_x = h_y = \frac{2\pi}{16}\varepsilon$ and time step $\Delta t = 1/50$. The reference solution is obtained by our method with the same mesh size but using a very fine time step, i.e., $\Delta t = 1/100 \varepsilon$. Table (3) shows the spatial errors of the wave function and the position density at time $T = 0.4$ for different ε . Here the position density error is not calculated for cumulative function but for the position density itself. Figure (3) presents the density's contour plot obtained with large Δt for different $\varepsilon = 1/32, 1/64, 1/128$ (rows from top to bottom with each row corresponding to the same ε) at different times $t = 0.4, 0.8$, and the the second and the forth columns are reference densities computed with very fine Δt . Results shown in Table (3) and Figure (3) confirm that our method can capture the correct observables with large time step and the spatial errors coincide our analysis given in Theorem (3.2).

Table 3: Spatial errors computed with $\Delta x = \frac{2\pi}{16}\varepsilon$ and a fixed time step $\Delta t = 1/50$ for different ε in Example 4.2. Reference solution is obtained with the same mesh size $\Delta x = \frac{2\pi}{16}\varepsilon$ and a fine time step $\Delta t = \varepsilon/100$.

ε	1/16	1/32	1/64	1/128
E_u	4.7093E-06	7.3482E-06	1.3777E-05	2.7109E-05
E_n	1.0472E-06	1.0528E-06	1.2366E-06	1.3789E-06

Example 4.3. Simulation of a 3D system

The last example we want to study is a 3D model, which is the most physics relevant, since most magnetic effects of quantum systems take place in the 3D space, which in general can not be reduced to lower dimensional subspaces.

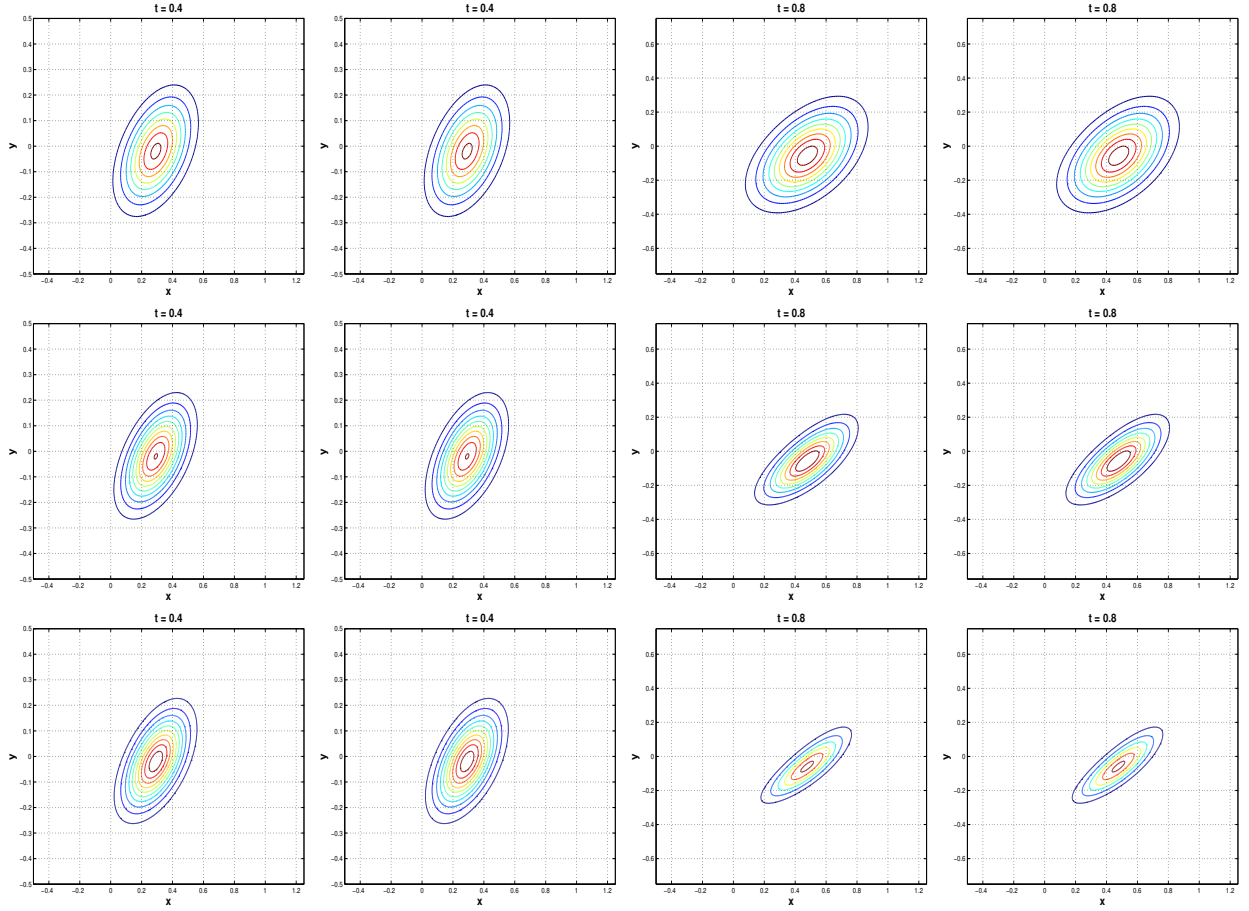


Figure 3: Contour plot of the density computed with $\Delta t = 1/50$ at different times $t = 0.4, 0.8$ for $\varepsilon = 1/32, 1/64, 1/128$ (rows from top to bottom) in Example 4.2, where the second and the fourth columns are reference solutions.

It is worth pointing out that the model (1.1) we have studied is highly related to the Pauli equation, which describes quantum evolution of spin-half particles in an external electromagnetic field. In an electromagnetic field described by the vector potential \mathbf{A} and scalar electric potential $V(x)$, the Pauli equation reads as

$$i\varepsilon\partial_t\mathbf{u}^\varepsilon = \left[\frac{1}{2}(-i\varepsilon\nabla - \mathbf{A})^2 + V(x)\right]\mathbf{I}\mathbf{u}^\varepsilon - \frac{1}{2}(\boldsymbol{\sigma} \cdot \mathbf{B})\mathbf{u}^\varepsilon, \quad (4.63)$$

where $\boldsymbol{\sigma} = (\sigma_x, \sigma_y, \sigma_z)$ are the Pauli matrices and $\mathbf{u}^\varepsilon = (u_+^\varepsilon, u_-^\varepsilon)^T$ is the two-component spinor wave function. Here, \mathbf{I} is the 2×2 identity matrix which acts as an identity operator and $\mathbf{B} = \nabla \times \mathbf{A}$ is the magnetic field.

The last term of (4.63), the so-called Stern-Gerlach term, leads to the anomalous Zeeman effect. If we drop this Stern-Gerlach term and consider a simplified version:

$$i\varepsilon\partial_t\mathbf{u}^\varepsilon = \left[\frac{1}{2}(-i\varepsilon\nabla - \mathbf{A})^2 + V(x)\right]\mathbf{I}\mathbf{u}^\varepsilon. \quad (4.64)$$

Then, \mathbf{u}^ε can be decoupled and the equation for each component takes the same form as (1.1).

In this test, we study a 3D system with constant magnetic field $\mathbf{B} = B(0, 0, 1)^T$. The vector potential is chosen as $\mathbf{A} = \frac{B}{2}(-y, x, 0)^T$ and we choose a homogeneous scalar potential, i.e., $V = 0$. The initial wave function is chosen as a double-well function with $O(\varepsilon)$ oscillation in phase, i.e.,

$$u_0(x, y, z) = (e^{-20(x-x_0)^2-20y^2-20z^2} + e^{-20(x+x_0)^2-20y^2-20z^2})e^{i\sin(y)\sin(z)/\varepsilon}, \quad (4.65)$$

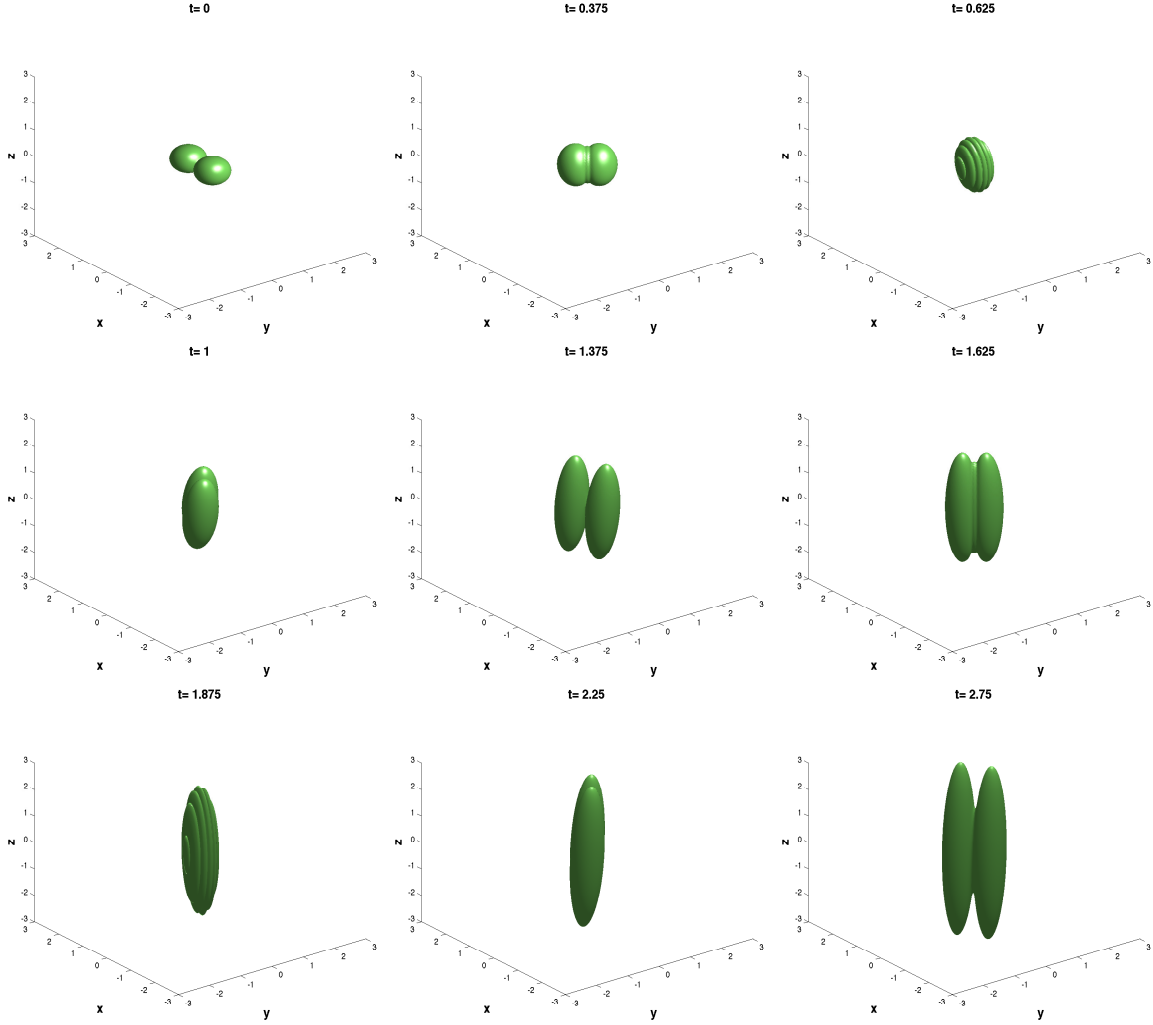


Figure 4: Isosurface of the density, $n(x, y, z) = 10^{-4}$, at different times for $\varepsilon = 1/16$ in Example 4.3.

with $x_0 = 0.5$. The computation domain is chosen as $[-4, 4]^3$. Here, we numerically compute the density evolution for $\varepsilon = 1/16$ with mesh size $h_x = h_y = h_z = \frac{1}{32}$ and time step $\Delta t = 1/40$.

Figure 4 presents the density's isosurface, $n(\mathbf{x}) = 10^{-4}$, at different times.

5. Conclusions and future directions

In this paper, we have proposed and analyzed a new time splitting spectral method for the semi-classical Schrödinger equation with vector potentials, where the NUFFT technique is applied in the interpolation step of the semi-Lagrangian method for the convection part. We have analyzed stability and accuracy of this method in approximating the wave function and in computing physical observables. Various numerical tests in one dimensional and up to three dimensional cases have been shown to verify the analytical results.

The semi-classical Schrödinger equation in electromagnetic field itself is of great significance both in theory and in applications, and studies of this model prepare us well for more complicated and important quantum mechanical models. For example, by incorporating the Stern–Gerlach term, the Schrödinger equation becomes the Pauli equation, which is the quantum wave equation for spinors. Also, if the wave function

models the quantum state of a charged particle, one can consider self-induced field by coupling the current equation with the Poisson equation or the Maxwell equations.

Acknowledgments

We acknowledge the support from the ANR-FWF Project Lodiquas ANR-11-IS01-0003, the Schrödinger Fellowship J3784-N32, the ANR project Moonrise ANR-14-CE23-0007-01 and the Natural Science Foundation of China grants 11261065, 91430103 and 11471050 (Y. Zhang), support from the NSF Grant RNMS (Ki-Net) 1107444 (Z. Zhou), the NSF grant DMS-1522184, DMS-1107291: RNMS (KI-Net) and Natural Science Foundation of China grant 91330203 (Z. Ma).

Appendix A. Proof of mass and energy conservation

In this appendix, we briefly present the proof for mass and energy conservation. We assume the wave function lies in Schwartz space $S(\mathbb{R}^d)$ hereafter.

Mass conservation.

Proof. For $u^\varepsilon \in C(\mathbb{R}_t; L^2(\mathbb{R}^d))$, first we note that $(-i\varepsilon\nabla - \mathbf{A})$ is a self-adjoint operator, i.e.,

$$\langle (-i\varepsilon\nabla - \mathbf{A})f, g \rangle = -i\varepsilon\langle \nabla f, g \rangle - \langle \mathbf{A}f, g \rangle = \langle f, (-i\varepsilon\nabla - \mathbf{A})g \rangle. \quad (\text{A.1})$$

Direct calculation confirms that

$$\frac{d}{dt}\|u^\varepsilon\|_{L^2} = \frac{d}{dt}\langle u^\varepsilon, u^\varepsilon \rangle = \langle \partial_t u^\varepsilon, u^\varepsilon \rangle + \langle u^\varepsilon, \partial_t u^\varepsilon \rangle = 0.$$

Energy conservation. □

Proof. Taking derivative for $\mathcal{E}(t)$, we have

$$\frac{d}{dt}\mathcal{E}(t) = (I) + (II),$$

where

$$\begin{aligned} (I) &:= \frac{1}{2}\langle (-i\varepsilon\nabla - \mathbf{A})\partial_t u^\varepsilon, (-i\varepsilon\nabla - \mathbf{A})u^\varepsilon \rangle + \frac{1}{2}\langle (-i\varepsilon\nabla - \mathbf{A})u^\varepsilon, (-i\varepsilon\nabla - \mathbf{A})\partial_t u^\varepsilon \rangle, \\ (II) &:= \langle \partial_t u^\varepsilon, Vu^\varepsilon \rangle + \langle u^\varepsilon, V\partial_t u^\varepsilon \rangle. \end{aligned}$$

Using the fact that $(-i\varepsilon\nabla - \mathbf{A})$ is a self-adjoint operator, we have

$$\begin{aligned} (I) &= \frac{1}{2}\langle (-i\varepsilon\nabla - \mathbf{A}) \left(\frac{1}{2i\varepsilon}(-i\varepsilon\nabla - \mathbf{A})^2 u^\varepsilon + \frac{V}{i\varepsilon}u^\varepsilon \right), (-i\varepsilon\nabla - \mathbf{A})u^\varepsilon \rangle \\ &\quad + \frac{1}{2}\langle (-i\varepsilon\nabla - \mathbf{A})u^\varepsilon, (-i\varepsilon\nabla - \mathbf{A}) \left(\frac{1}{2i\varepsilon}(-i\varepsilon\nabla - \mathbf{A})^2 u^\varepsilon + \frac{V}{i\varepsilon}u^\varepsilon \right) \rangle \\ &= \frac{1}{2}\langle \frac{1}{2i\varepsilon}(-i\varepsilon\nabla - \mathbf{A})^2 u^\varepsilon + \frac{V}{i\varepsilon}u^\varepsilon, (-i\varepsilon\nabla - \mathbf{A})^2 u^\varepsilon \rangle \\ &\quad + \frac{1}{2}\langle (-i\varepsilon\nabla - \mathbf{A})^2 u^\varepsilon, \frac{1}{2i\varepsilon}(-i\varepsilon\nabla - \mathbf{A})^2 u^\varepsilon + \frac{V}{i\varepsilon}u^\varepsilon \rangle \\ &= \frac{1}{2i\varepsilon}\langle Vu^\varepsilon, (-i\varepsilon\nabla - \mathbf{A})^2 u^\varepsilon \rangle - \frac{1}{2i\varepsilon}\langle (-i\varepsilon\nabla - \mathbf{A})^2 u^\varepsilon, Vu^\varepsilon \rangle. \end{aligned}$$

Similarly,

$$\begin{aligned} (II) &= \langle \frac{1}{2i\varepsilon}(-i\varepsilon\nabla - \mathbf{A})^2 u^\varepsilon + \frac{V}{i\varepsilon}u^\varepsilon, Vu^\varepsilon \rangle + \langle Vu^\varepsilon, \frac{1}{2i\varepsilon}(-i\varepsilon\nabla - \mathbf{A})^2 u^\varepsilon + \frac{V}{i\varepsilon}u^\varepsilon \rangle \\ &= \frac{1}{2i\varepsilon}\langle (-i\varepsilon\nabla - \mathbf{A})^2 u^\varepsilon, Vu^\varepsilon \rangle - \frac{1}{2i\varepsilon}\langle Vu^\varepsilon, (-i\varepsilon\nabla - \mathbf{A})^2 u^\varepsilon \rangle = -(I). \end{aligned}$$

Therefore, we have $(I) + (II) = 0$, which implies directly that $\mathcal{E}(t) = \mathcal{E}(0)$. □

References

- [1] J. Avron, I. Herbst and B. Simon, Schrödinger operators with magnetic fields. I. General interactions, *Duke Math. J.* 45 (1978) 847-883.
- [2] W. Bao, S. Jiang, Q. Tang and Y. Zhang, Computing the ground state and dynamics of the nonlinear Schrödinger equation with nonlocal interactions via the nonuniform FFT, *J. Comput. Phys.* 296 (2015) 72-89.
- [3] W. Bao, S. Jin and P.A. Markowich, Time-splitting spectral approximations for the Schrödinger equation in the semiclassical regime, *J. Comput. Phys.* 175 (2002) 487-524.
- [4] W. Bao, S. Jin and P.A. Markowich, Numerical studies of time-splitting spectral discretizations of nonlinear Schrödinger equations in the semiclassical regime, *SIAM J. Sci. Comput.* 25 (2003) 27-64.
- [5] W. Bao, Q. Tang and Y. Zhang, Accurate and efficient numerical methods for computing ground states and dynamics of dipolar Bose-Einstein condensates via the nonuniform FFT, *Commun. Comput. Phys.* 19 (5) (2016) 1141-1166.
- [6] S. Blanes, F. Casas, J.A. Oteo and J. Ros, The Magnus expansion and some of its applications, *Phys. Rep.* 470 (2009) 151-238.
- [7] S. Blanes, F. Diele, C. Marangi and S. Ragni, Splitting and composition methods for explicit time dependence in separable dynamical systems, *J. Comput. Appl. Math.* 235 (2010) 646-659.
- [8] A. Dutt and V. Rokhlin, Fast Fourier transforms for nonequispaced data, *SIAM J. Sci. Comput.* 14 (1993) 1368-1393.
- [9] B. Engquist and O. Runborg, Computational high frequency wave propagation, *Acta Numer.* 12 (2003) 181-266.
- [10] E. Faou, V. Gradinaru and Ch. Lubich, Computing semiclassical quantum dynamics with Hagedorn wavepackets, *SIAM J. Sci. Comput.* 31(2009) 3027-3041 .
- [11] V. Gradinaru and G.A. Hagedorn, Convergence of a semiclassical wavepacket based time-splitting for the Schrödinger equation, *Numer. Math.* 126 (2013) 1-21 .
- [12] L. Greengard and J-Y. Lee, Accelerating the nonuniform fast Fourier transform, *SIAM Rev.* 46 (2004) 443-454.
- [13] G.A. Hagedorn, Raising and lowering operators for semi-classical wave packets, *Ann. Phys.* 269 (1998) 77-104 .
- [14] E.J. Heller, Time dependent approach to semiclassical dynamics, *J. Chem. Phys.* 62 (1975) 1544-1555 .
- [15] S. Jiang, L. Greengard and W. Bao, Fast and accurate evaluation of nonlocal Coulomb and dipole-dipole interactions via the nonuniform FFT, *SIAM J. Sci. Comput.* 36 (2014) B777-B794.
- [16] S. Jin and X. Li, Multi-phase computations of the semiclassical limit of the Schrödinger equation and related problems: Whitham vs Wigner, *Phys. D: Nonlinear Phenom.* 182 (2003) 46-85.
- [17] S. Jin, P. A. Markowich and C. Sparber, Mathematical and computational methods for semiclassical Schrödinger equations, *Acta Numer.* 20 (2011) 121-209 .
- [18] S. Jin and S. Osher, A level set method for the computation of multi-valued solutions to quasi-linear hyperbolic PDE's and Hamilton-Jacobi equations, *Commun. Math. Sci.* 1 (2003) 575-591.
- [19] S. Jin, H. Wu and X. Yang, Gaussian beam methods for the Schrödinger equation in the semi-classical regime: Lagrangian and Eulerian formulations, *Commun. Math. Sci.* 6 (2008) 995-1020.
- [20] S. Jin, H. Wu and X. Yang, Semi-Eulerian and high order Gaussian beam methods for the Schrödinger equation in the semiclassical regime, *Commun. Comput. Phys.* 9 (2011) 668-687.
- [21] S. Jin and Z. Zhou, A semi-Lagrangian time splitting method for the Schrödinger equation with vector potentials, *Communications in Information and Systems* 13 (2013) 247-289.
- [22] H. Liu, O. Runborg and Tanushev, Error estimates for Gaussian beams, *Math. Comp.* 82 (2013) 919-952 .
- [23] M. M. Popov, A new method of computation of wave fields using Gaussian beams, *Wave Motion* 4 (1982) 85-97.
- [24] J. Qian and L. Ying, Fast Gaussian wave pack transforms and Gaussian beams for the Schrödinger equation, *J. Comput. Phys.* 229 (2010) 7848-7873.
- [25] J. Ralston, Gaussian beams and the propagation of singularities, *Studies in partial differential equations* 23 (1982) 206-248.
- [26] G. Russo and P. Smereka, The Gaussian wave packet transform: Efficient computation of the semi-classical limit of the Schrödinger equation. Part 1-Formulation and the one dimensional case, *J. Comput. Phys.* 233 (2013) 192-209.
- [27] G. Russo and P. Smereka, The Gaussian wave packet transform: Efficient computation of the semi-classical limit of the Schrödinger equation. Part 2. Multidimensional case, *J. Comput. Phys.* 257 (2014) 1022-1038.
- [28] J. Shen and T. Tang, *Spectral and High-Order Methods with Applications*, Science Press, Beijing, 2006.
- [29] M.O. Scully and M.S. Zubairy, *Quantum optics*, Cambridge University Press (1997).
- [30] E. Süli and A. Ware, A spectral method of characteristics for hyperbolic problems, *SIAM J. Appl. Math.* 28 (1991) 423-445.
- [31] N.M. Tanushev, Superpositions and higher order Gaussian beams, *Commun. Math. Sci.* 6 (2008) 449-475.
- [32] D. Yin and C. Zheng, Gaussian beam formulation and interface conditions for the one-dimensional linear Schrödinger equation, *Wave Motion* 48 (2011) 310-324.
- [33] Z. Zhou, Numerical approximation of the Schrödinger equation with the electromagnetic field by the Hagedorn wave packets, *J. Comput. Phys.* 272 (2014) 386-40.